EFFECT OF PARTICLE ALIGNMENT ON MECHANICAL PROPERTIES OF NEAT CELLULOSE NANOCRYSTAL FILMS

*ALEXANDER B. REISING, ROBERT J. MOON, JEFFREY P. YOUNGBLOOD**

ABSTRACT

Shear-based film casting methods were used to cast neat films from wood-based cellulose nanocrystal (CNC) suspensions. The degree of CNC alignment in dried films was characterized using the Hermans order parameter (S), and the film elastic modulus (E), ultimate tensile strength (σ_f), elongation at failure (ε_f), and work of fracture (WF) were measured with respect to casting direction and CNC alignment. The degree of CNC alignment in dried films was found to increase with higher casting shear rates (0, $10 \cdot s^{-1}$, and $100 \cdot s^{-1}$) and at higher suspension pH (~3 versus ~7). The maximum orientation (S=0.53) was achieved for CNC suspensions having a neutral pH and sheared at a rate of $100 \cdot s^{-1}$. Elastic modulus of CNC films scaled with CNC alignment reached a maximum average of E= 30 GPa in the direction of CNC alignment. σ_f, ε_f, and WF did not scale with CNC alignment. Thermal treatments (85°C for 24 h) to CNC films had minimal influence on E, σ_f, ε_f, and WF.

INTRODUCTION

Cellulose nanomaterials (CN) are nanoparticles extracted from various cellulose sources (non-woody plants, trees, algae, tunicates, and some species of bacteria) and are being studied for uses in composites [1]. The morphology and properties of the resulting CNs depend on cellulose source and extraction method and will have an impact on composite processing and properties [1]. Bacterial cellulose (BC) is made up of ribbon-like fibres (~6–50 nm in diameter, microns in length) in a dense network mat called a *pellicle*, which is subsequently mechanically or chemically treated to modify the network structure [1,2]. Mechanical extraction methods for plant or tree cellulose source materials typically produce fibrillar cellulose particles, one type of which is called cellulose nanofibres (CNFs), which are typically 4–20 nm in diameter, microns in length, and can have a branched structure. Chemical extraction methods from a given cellulose source generally use sulphuric-acid hydrolysis [1,3–5] and produce cellulose nanocrystals (CNCs) that are in an aqueous colloidal suspension stabilized by negatively charged sulphate ester groups on the particle surface. The CNCs are rod-like particles with a high aspect ratio and are composed of a high fraction of crystalline cellulose. Variations in the extraction method (and the cellulose source material) can alter CNC length, length polydispersity, aspect ratio, and surface charge, all of which affect suspension rheology, pH, agglomeration, and mesophase formation behaviors [6–11]. For example, CNCs from wood are typically 3–5 nm in diameter and 50–500 nm in length, while CNCs from tunicates are typically 8–20 nm in diameter and 100–4000 nm in length. The mechanical properties of CNCs are anisotropic, being higher in the direction parallel to the CNC length (elastic modulus, E = 100–220 GPa [1,12] and ultimate tensile strength, σ_f =7.5 GPa [13]), as compared to directions perpendicular to the CNC length (E=3–50 GPa [1,12]). This property anisotropy results from the anisotropy of

ALEXANDER B. REISING
School of Materials Engineering, Purdue University, 701 W. Stadium Ave., West Lafayette, IN, 47907
USA

ROBERT J. MOON
The Forest Products Laboratory. US Forest Service, 1205 W. State Street, West Lafayette, IN 47907-2057,
USA

JEFFREY P. YOUNGBLOOD
School of Materials Engineering, Purdue University, 701 W. Stadium Ave., West Lafayette, IN, 47907
USA
*Contact: jpyoungb@purdue.edu

stacking of the cellulose chains that make up the monoclinic crystalline structure of cellulose, in which the cellulose chains run parallel to the long axis of the CNC.

The excellent mechanical properties of crystalline cellulose, which are better than those of Kevlar [1,3–5], have prompted research into CN use in composite manufacturing. Most of this research has focused on low concentrations of CNs (less than 30 wt%) to act as a reinforcement phase in polymer matrix composites [1,3–5], while only a few studies have investigated free-standing neat CN films (100% CNs) that are self-supporting [1]. Neat CN films are typically produced by solution-casting techniques [1,14], resulting in transparent films that are tens of microns thick and have a random CNC orientation within the film plane. The mechanical properties of neat CN films have been measured for CNC extracted from wood (E= 6 GPa) [14] and from tunicates (E= 5–10 GPa, σ_f =40–70 MPa, strain to failure ε_f =0.5–5%, work of fracture WF=2.8 MJ/m^3) [15,16] and are comparably lower than those of neat films produced by CNF (E= 6–15 GPa, σ_f =95–312 MPa, ε_f =2–11%, WF=1–15 MJ/m^3) [1,17–21] and BC (E= 10–35 GPa, σ_f =87–510 MPa, ε_f =1.1–4.4%, WF=0.4–12 MJ/m^3) [1,2,22–28]. The mechanical properties of neat CN films are lower than those of individual CN particles because of several factors such as ineffective load transfer caused by porosity and weak CN-CN interfaces within the films.

Because of the strongly axial properties and high particle aspect ratio of CNs, preferentially aligning the particles within a composite should increase the properties in the aligned direction. Several methods have been used to induce CN alignment within composites: magnetic fields [29–34], electric fields [35–37], mechanical shearing of CNC suspensions [29,38–40], combined field and mechanical shearing [41], drawing of as-cast CN films [22,42] and cellulose-cellulose composites [43], and wet-spinning of CN composite fibres [44]. The magnetic fields do not orient individual CNCs uniaxially, but instead orient the chiral nematic domain axes of the CNC mesophase, with the CNCs oriented perpendicular to magnetic field lines [29]. Therefore, it may be challenging to produce composites with complete CNC alignment in a single direction (i.e., 1-D). In AC electric fields, individual CNCs align in the field direction, the extent of alignment depending on CNC size, surface charge, field strength, and frequency [35], which offers the possibility of producing composites with 1-D CNC alignment. Shear-based methods for CNC suspensions can orient individual CNCs uniaxially in the direction of shear. However, retaining the CNC alignment in the final dried CNC films is challenging. A time- and rheology-dependent relaxation occurs once shear is removed, and the uniaxial CNC alignment dissipates [29]. To counter this relaxation, Orts et al. demonstrated that longer CNC particles could be used [29]. Alternatively, Nishiyama et al. cast CNC films under constant rotational shearing until the film was dried and achieved near-complete uniaxial orientation (0.96 Hermans order parameter) [39]. However, the resulting dried film was cylindrical, which severely limits potential applications and complicates mechanical-property characterization. Neither study investigated the role of CNC alignment on the resulting mechanical properties of the dried films. Bohn et al. used drawing methods to pull semi-dry BC films into alignment and held the strain during drying, resulting in upwards of ~80% BC alignment depending on drawing strain and drying treatment [22]. The mechanical properties increased with BC alignment and resulted in more than doubling of E (up to 25 GPa) and σ_f (up to 581 MPa) in the BC aligned direction. Similarly, Gindl and Keckes [43] mechanically stretched solution-cast all-cellulose composites and reported a three-fold increase in E (up to 33 GPa) and a doubling of σ_f (up to 430 MPa) in the aligned direction. For wet-spinning, the flow profiles resulted in CNC alignment with the long axis along the length of the spun fibre, with an orientation index of up to 0.72 [44]. These studies suggest that by developing CNC alignment in neat CNC films, it may be possible to increase the mechanical properties in the aligned direction.

The objective of the current study is to investigate the role of CNC alignment on the resulting tensile properties (E, σ_f, ε_f, and WF) of neat CNC films from wood-based CNCs. A shear-based casting technique was used to induce CNC alignment within the films, in which the influence of casting shear rate and CNC suspension pH on the resulting CNC alignment within dried films was investigated.

MATERIALS AND METHODS

Preparation of Cellulose Nanocrystal Suspensions

Cellulose Nanocrystal Extraction - The CNC extraction process was carried out at the USDA Forest Service-Forest Products Laboratory, Madison, WI. CNCs were extracted through sulphuric-acid hydrolysis of microcrystalline cellulose (MCC) (FMC BioPolymer; Lattice® NT-020) following procedures described by Beck-Candanedo et al. [8]. The hydrolysis (64% sulphuric acid, 8 to 1 acid to MCC weight ratio, 45°C, 60 minutes) was followed by quenching with deionized water, centrifuge rinsing, washing, and then dialysis for approximately one week to remove the remaining acid. The suspension was then ultrasonicated to disperse the CNCs through mechanical agitation and centrifuged a final time for macroparticle removal. The resulting CNC suspension was 1.3 wt% CNCs in water having a pH of 2.9.

Suspension Modification - To study the effects of suspension pH on CNC film processing, acid and base titrations were used to alter the pH of the "as-received" CNC suspension. A "neutral" pH CNC suspension was produced by the addition of dilute KOH until a pH of 6.4 was reached. The resulting suspension was dialyzed against pure deionized water for 24 hours to remove excess ions from the suspension. Unexpectedly, the pH decreased from 6.4 to 4.3, suggesting that the CNCs in suspension were inherently acidic, although the reason for this is unclear. As

a result, more dilute KOH was added, increasing the pH to 6.35, and excess ions were not removed from the suspension. The two suspensions used in the current study are labelled as CNC-l for low pH (pH 2.9, 1.3 wt% CNCs), and CNC-n for neutral pH (pH 6.4, 1.3 wt% CNCs).

Before shear casting, the suspensions were concentrated to a viscous, gel-like state using a Yamato RE500 rotary evaporator at 38°C and 20 Torr. The critical CNC concentration of the gel-like state was qualitatively assessed as being the lowest CNC concentration at which the CNC gel would stick to the bottom of a 1 cm diameter flask (as opposed to flowing into the cap) after it was turned upside down. The critical CNC concentration was 10.3 wt% and 7.5 wt% for the CNC-l and CNC-n suspensions respectively.

Preparation of Neat Cellulose Nanocrystal Films

Random Films - A film casting method was used to produce CNC films with a random in-plane CNC orientation (Fig. 1 (top)). CNC suspensions (1.3 wt% CNC) were poured into flat polystyrene (PS) Petri dishes, uniformly filling the dishes halfway, and were left to dry at ambient conditions (27°C and 50% relative humidity, RH) for several days. The CNC alignment induced by pouring and spreading of the suspensions was believed to have been minimized by using suspensions with CNC concentrations (e.g., 1.3 wt. % CNC) that were well below the critical gel-like concentration. Once dry, the resulting films were carefully pried off the PS dish with a razor blade. These unsheared films contained no wrinkles or curvature. However, there was a thickness gradient, with the thinnest portion (~10 µm thick) along the outer edge and the thickness increasing uniformly towards the centre of the film (~120 µm thick). Testing strips were therefore cut perpendicular to the film radii, resulting in the least possible thickness variation.

Shear-Cast Films - A shear film-casting method [45] was used to induce CNC alignment within the final dried films (Fig. 1 (bottom)). The CNC suspensions were just below the critical CNC concentration where the suspension transformed into a viscous, gel-like state (10.3 wt% and 7.5 wt% for CNC-l and CNC-n respectively). It is assumed here that shear casting of "high"-viscosity CNC suspensions restricts CNC rotational diffusion (*i.e.*, CNC re-orientation) that may occur while the as-cast suspension sits following shearing. This helps to lock in the CNC alignment induced by shearing and maintains this alignment in the final dried film, yet still provides the fluidity necessary for wetting to the surface and not being pulled off by the blade. For shear casting, a standard laboratory-scale tape-casting apparatus (custom-built by EPH Engineering Associates, Inc., with a Bug-O Systems Bug-0343 motor) having an adjustable speed control for the doctor blade (a stainless-steel blade with a bottom edge defined by a 45-degree taper to a fine edge) was used. Shear rates were calculated from the speed of the doctor blade and the casting-gap depth. Shear-cast neat films (100% CNCs) of uniform thickness were produced using an assembly that consisted of a glass casting surface with two polyethylene terephthalate (PET, 0.60 mm thick) strips attached, spaced 30 mm apart, creating a channel inside which to cast the films. CNC suspensions (~1.2 mL) were pipetted onto the glass substrate between the PET strips. The doctor blade was balanced evenly on the PET strips, spanning the gap to produce an even casting level, and the suspension between the strips was sheared by the doctor blade at set casting rates ($10 \cdot s^{-1}$ and $100 \cdot s^{-1}$). After the initial shearing, an additional ~1–2 mL of CNC suspension was pipetted on top of the freshly cast film (between the PET strips), and the shearing process was repeated. This process was repeated until a total of six shearing passes had been completed. The film was then allowed to sit at ambient conditions (27°C and 50% RH) and once sufficiently "dry" (~2 h), the film edges in contact with the PET strips were cut away and the film delaminated from the glass surface. The resulting films were ~41 µm thick. One film was cast for each casting condition listed in Table 1. The CNC alignment of each film was measured using X-ray diffraction, and the sample was subsequently cut into smaller test samples for tensile testing.

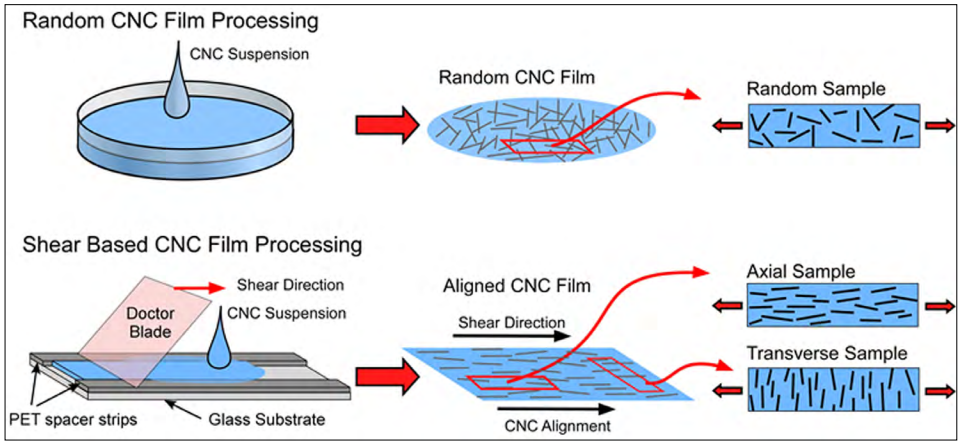

Fig. 1 - Schematic of CNC film processing and configuration of the test samples extracted as cast films for (top) unsheared and (bottom) shear casting. Processing without shear produced films with minimal CNC alignment. The shear-based processing produced films with CNC alignment in the shear direction. Mechanical testing of the films was carried out for two orthogonal cases, parallel to the direction of CNC alignment (axial samples), and perpendicular to the CNC alignment (transverse sample).

Heat Treatment - Additional test samples were cut from the original CNC film cast from the CNC-n at $100 \cdot s^{-1}$ shear-rate conditions and were heated in a drying oven at 85°C for 24 h. They were then equilibrated at ambient conditions (27°C and 50% RH) for at least 24 h before subsequent

Fig. 2 - TEM images of CNC suspension deposited on a TEM grid.

testing. The density of each sample was measured before and after heat treatment.

Transmission Electron Microscopy

A Philips CM-100 transmission electron microscope (TEM) at 100kV, spot 3, 200 µm condenser aperture, and 50 µm objective aperture, calibrated using a replica grating, was used to characterize the morphology of individual CNC particles. CNC particles were deposited on a TEM grid (400 mesh Formvar/carbon filmed grid prepared by blow discharge) by floating the grid on CNC suspension droplets (~0.05 wt% concentrations) for ~2 minutes, then rinsing through 2% aqueous uranyl acetate, staining, and blotting dry. The length and width of 225 particles were measured using ImageJ of TEM images (with contrast enhanced to identify CNC edges clearly). Only clearly identifiable individual crystals were measured. The measured CNC particle size (Fig. 2) had an average length of 129 nm (1 standard deviation, SD = 76 nm), a width of 7.9 nm (SD = 2.5 nm) and an aspect ratio of 22 (SD = 13 nm).

Zeta Potential

Zeta potential measurements were completed using a Malvern Zetasizer Nano-Z. The as-received CNC suspension was diluted to 0.1 wt% CNC by adding nanopure water, producing a suspension that was transparent, homogeneous, and had a pH=5.1. This "initial" suspension was then equally divided into two smaller batches to produce a range of solutions having pH values from 1 to 15. One of the batches was used to prepare 50 ml solutions with adjusted pH values from 5 to 1 by adding HCl, while the other batch was used to prepare 50 ml solutions with pH values from pH 5 to 14 by adding NaOH. For each of these solutions, 20 ml was used for surface charge analysis.

Orientation Quantification

The CNC alignment in the dried films was characterized by two-dimensional (2D) wide-angle X-ray diffraction (WAXD, Bruker GADDS X-Ray Diffractometer, Cu K(alpha) source, with a three-circle goniometer and a 2D HiStar area detector, 30 kV accelerating voltage, 40 mA current, 0.5 mm pinhole collimator / 546 nm wavelength monochromator). Scans were taken for 1800 seconds each at a distance of 6.080 cm from the detector, with films mounted perpendicular to the X-ray beam. WAXD measures the diffracting X-rays off a given sample as a function of the diffraction angle (2θ) with respect to the direction of the primary X-ray beam. The resulting 2D diffraction pattern consists of Debey-Scherrer rings, which gives the azimuthal intensity distribution for each 2θ diffraction peak. Diffracted X-ray intensities were measured with respect to the shearing direction used in casting the films. Based on methods conducted by Nishiyama et al. [39], the intensity

TABLE 1 *CNC neat film properties.*

Samples	Suspension Concentration (wt%)	S	Film Density (g/cm³)	E (GPa) A	E (GPa) T	σ_f (MPa) A	σ_f (MPa) T	ε_f (%) A	ε_f (%) T	WF (MJ/m³) A	WF (MJ/m³) T
CNC-l Unsheared	1.3	0.04	1.43 (0.11)	14.9 (1.4)	--	70 (29)	--	0.6 (0.3)	--	0.26 (0.19)	--
10 s^{-1}	10.3	0.27	xx	21.6 (0.2)	8.5 (1.4)	61 (21)	45 (12)	0.3 (0.1)	0.7 (0.2)	0.13 (0.09)	0.18 (0.11)
100 s^{-1}	10.3	0.36	1.55 (0.02)	23 (2.1)	7.2 (0.7)	49 (8)	46 (11)	0.4 (0.4)	0.9 (0.3)	0.10 (0.04)	0.21 (0.11)
CNC-n 100 s^{-1}	7.5	0.53	1.55 (0.02)	29.7 (1.2)	6.7 (0.2)	77 (10)	48 (2)	0.3 (0.1)	0.9 (0.2)	0.12 (0.04)	0.23 (0.04)
CNC-n w/ heat 100 s^{-1}	7.5	0.53	1.55 (0.02)	31.5 (0.5)	7.0 (0.8)	70 (6)	36 (13)	0.2 (0.03)	0.6 (0.3)	0.09 (0.01)	0.18 (0.04)

S= Hermans Order Parameter.
A= axial – parallel to the direction of shear, T= transverse – perpendicular to the direction of shear.
Numbers in brackets () are 1 standard deviation

distribution after background subtraction of the (200) plane diffraction (at 2θ ≈ 21° for the monoclinic cellulose unit cell as described by Wada et al. [46]) was used for calculation of a Hermans order parameter, S, for each film, using the equation

$$S = \frac{1}{2}(3\{\cos^2\phi\} - 1), \quad (1)$$

where

$$\{\cos^2\phi\} = \frac{\sum_0^{\pi/2} I(\phi)\cos^2\phi \sin\phi \, \Delta\phi}{\sum_0^{\pi/2} I(\phi)\sin\phi \, \Delta\phi}, \quad (2)$$

in which ϕ is the azimuthal angle with respect to the film-shearing direction at ϕ = 0 and I(ϕ) is the (200) plane diffracted intensity at ϕ.

Density

The density of each tensile specimen was measured. Tensile specimens were stored at, and all measurements (mass and dimensions) were completed under, ambient conditions (27°C and 50% RH). Film masses were measured using a microbalance with ±1 μg resolution, while the dimensions were measured with a micrometer and averaged. The film thicknesses were measured four to six times across each film with ±1 μm precision and averaged. Film widths were measured three or four times across each film with ±5 μm precision and averaged. Film lengths were only measured once with ±10 μm precision.

Tensile Testing

Tensile stress-strain tests were conducted using a TA Instruments Q800 Dynamic Mechanical Analyzer (DMA) used in controlled force mode, by which E, σ_f, and ε_f of the CNC films were determined. The area under the stress-strain curves was integrated and used to estimate WF. The tensile tests were performed at 27°C and 50% RH using a 1.0 N/min load rate and an initial pre-load of 0.005 N. Each sheared film was sectioned into axial (parallel to the shear direction) and transverse (perpendicular to the shear direction) tensile specimens approximately 2 mm wide and 15–20 mm long. The film strips were then carefully mounted onto a thin steel-foil (80 μm thick) frame as shown in Fig. 3a. Superglue (Loctite®, control gel) was used to bond the tensile strip ends to the steel-frame assembly and left to cure for 24 h before testing. The gauge lengths for determining strain were measured with calipers as the distance between the steel tabs. Once mounted in the DMA, the steel assembly was cut (Fig. 3b) so that it was no longer a continuous strip between the grips and thus did not interfere with the tensile test. Five tensile specimens were tested. Samples failing at the tensile grip were not included in the data analysis; the results shown in Table 1 are averages based on three to five samples.

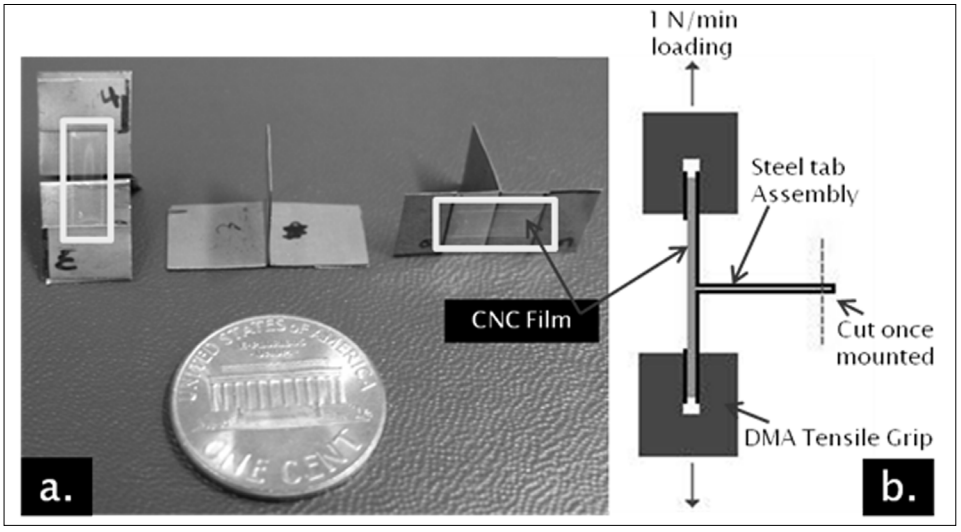

Fig. 3 - Mounted CNC films as DMA tensile testing specimens (a) and tensile test schematic (b). The CNC film (outlined by boxes) is super-glued between steel tabs and the steel support structure at the ends. Once mounted, the steel mount is cut along the dotted line, freeing the film for testing.

RESULTS AND DISCUSSION

Suspension Characterization

CNC Surface Charge and Sulphur Content - The "as-received" CNC suspension was characterized by zeta potential as a function of pH. At low pH (~2), a ~-30 mV potential was measured, and with increasing pH, the potential became more negative until it reached ~-60 mV and then stayed constant from a pH of ~3 to ~8.5. Additional increases in pH resulted in the potential becoming less negative monotonically to ~-30 mV at pH 12, giving the pH vs. zeta potential curve a "bathtub" shape. The more positive potentials at low pH may be explained by protonation of the sulphate ester groups. However, the cause of the more positive potentials at basic conditions is unclear, but they may be due to sulphate ester hydrolysis under base catalysis or an ionic strength effect due to added ions. Regardless, at the casting pH, both CNC-l and CNC-n had similar potentials of ~-50 to -60 mV respectively. As well, the CNC had a 0.92% surface sulphate content.

CNC Alignment Within Films

The X-ray diffraction-area detector scans demonstrated that the shear casting technique used in the current study resulted in CNC alignment with the dried film (Fig. 4). The unsheared CNC films exhibited a uniform diffraction pattern, with constant intensity at all azimuthal ϕ angles for any given 2θ peak, which is representative of a random CNC orientation within the plane of the film. For shear-cast films, the (200) planes diffracted more X-rays in azimuthal ϕ angles perpendicular to the shearing direction than in ϕ angles parallel to the shear direction, which is representative of in-film CNC alignment with the CNC long axis oriented parallel to the shear direction. The resulting values of Hermans order parameter, S, for these results are given in Table 1. The results demonstrate that the CNC alignment within the

shear-casting direction of the film could be increased by increased casting shear rate and higher suspension pH. The 2D WAXD technique used in the current study measures the average CNC alignment throughout the film thickness, and therefore it is unclear whether there is a distribution of CNC alignment as a function of position through the film thickness. It is unclear what effect, if any, such variations in orientation through the film thickness would have on the properties. Regardless, changes in mechanical properties as a function of average orientation will still indicate to what degree orientation affects the properties.

Shear-Rate Influence - The CNC alignment in the final films increased as the shear rate was increased. For the CNC-l unsheared sample, the CNC alignment was effectively 2D random with S= 0.04. By using shear casting, the CNC alignment was increased to S=0.27 with a shear rate of 10 s^{-1} and S=0.36 with a shear rate of 100 s^{-1}. This result is similar to that reported by Orts et al., who showed that the CNC order parameter increased linearly with the $\log_{10}$ of shear rate until reaching a plateau near 100·s^{-1} [29].

Suspension pH Influence - The current study has shown that increasing the pH from approximately 2.5 to 6.5 (i.e., "neutral" pH) resulted in stronger CNC alignment in the final dried film. The mechanism for this improved alignment is considered to involve changes in CNC-CNC interaction caused by changes in suspension pH. In general, suspension pH can modify the zeta potential between particles, which alters the electrostatic particle-particle interactions in accordance with DLVO theory (a theory named after Derjaguin, Landau, Verwey, and Overbeek that uses the combined effect of van der Waals and double-layer forces to describe the interaction between charged surfaces through a liquid medium) [47]. These changes in particle-particle interactions can then affect the suspension rheological properties. In the current study, the CNCs have a negative surface charge as a result of the remnant sulphate ester groups from sulphuric-acid hydrolysis. The surface charge should decrease as pH decreases because the increasing numbers of protons from the acid neutralize the negative charges. This reduction in charge was observed experimentally for the CNC suspensions; at a pH of ~7, the zeta potential was -60mV, while at a pH of 2, the zeta potential was -30mv. Note that the CNC suspensions at either pH (2 or 7) were stable colloidal dispersions. Changes to the CNC particle-particle charge interactions should subsequently change the rheological behavior of the CNCs within the suspension (*e.g.*, by rotational mobility of individual CNC particles facilitating their alignment to the shear flows) as well as orientation retention after shear ceases (*e.g.*, rotational diffusion). However, during casting, both CNC-l (pH≈3) and CNC-n (pH≈6.5) suspensions had similar potentials of ~-50 to -60 mV respectively, which means that the observed orientation differences may be dominated by other factors. It is also unclear why the slightly more negatively charged CNC-n surface has a higher gel-point concentration. Nonetheless, it is assumed here that the CNC rotational diffusion after shear was restricted by the increased suspension viscosity that occurred at the gel-like critical CNC concentration. Research by Araki et al. identified the formation of a new CNC suspension phase, beyond the liquid crystalline mesophases, in which CNC surface-charge repulsion led to a "birefringent glassy phase" in which CNCs were "frozen" into position, forming a viscous gel-like state with no coagulation [48]. The birefringent glassy phase was identified by the formation of a crosshatch pattern when viewed through crossed polarizers, as opposed to the typical Schlieren fingerprint texture observed for chiral nematic CNC mesophases. Both the CNC films exhibited a cross-hatched pattern when viewed through crossed polarizers (Fig. 5). We surmise that, when these suspensions were sheared, the glassy "frozen" microstructure was broken up and allowed the CNCs to orient with the shear direction. Once shear ceased, the order was once again "frozen" into position, preventing or limiting the relaxation identified by Orts et al. and allowing our films to dry

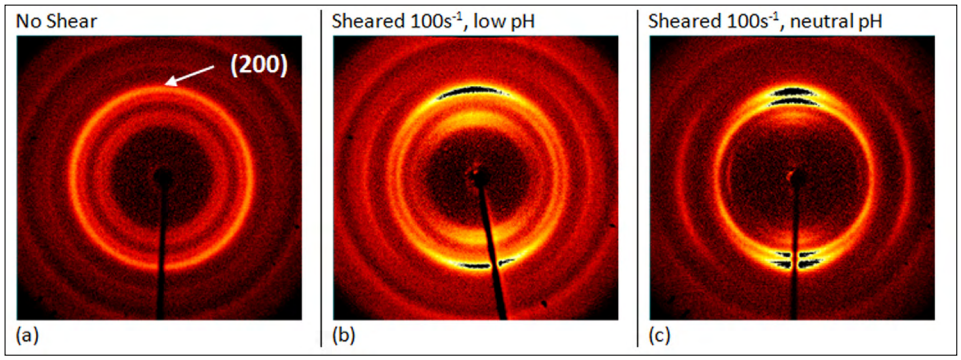

Fig. 4 - XRD area scans of CNC films showing the Debey-Scherrer rings. The (200) plane reflection is the most intense and varies with respect to CNC alignment within the film and with film orientation. (a) unsheared, (b) sheared at 100·s^{-1} with a low suspension pH, and (c) sheared at 100·s-1 with a neutral suspension pH. The shear casting direction is from right to left with respect to the scans.

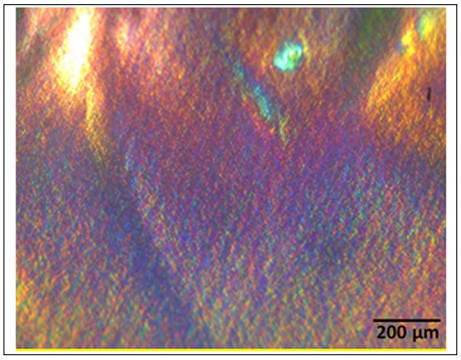

Fig. 5 - Optical micrographs of dried CNC sheared film (100 s^{-1}), taken in transmission mode through crossed polarizers. The cross-hatch pattern observed indicates the presence of a "birefringent glassy" phase of CNCs dominated by surface charge repulsion between crystals.

while retaining more of their shear-induced orientation.

CNC Film Properties

The measured E, σ_f, ε_f, and WF as a function of Hermans order parameter, S, of solution-cast neat CNC films are shown in Fig. 6. The tensile properties are influenced by several factors, including, but not limited to, film density, CNC properties, CNC length, CNC-CNC interface properties, moisture content, and CNC alignment. The focus of the current study and the subsequent discussion will be on the role of CNC alignment on tensile properties. CNC alignment influences film properties because of the property anisotropy of the individual CNC particles themselves. The highly ordered parallel stacking of cellulose chains in the direction of the CNC particle length results in higher mechanical properties in this direction (E= 100–220 GPa) as compared to the orthogonal directions (E=3–50 GPa) [1]. The results of the current study show that the degree of CNC alignment influenced E, but did not appear to influence σ_f, ε_f, or WF. The elastic-property anisotropy between the axial (parallel to the shear direction), E_A, and transverse (perpendicular to the shear direction), E_T, film directions are studied and discussed.

Film Density - The density of the neat CNC films produced by solution casting approached the theoretical density of crystalline cellulose (1.60 g/cm^3). The small particle size and strong surface interactions of individual CNCs enable the formation of a dense mat during solution casting. The unsheared films had densities (standard deviations) of 1.43 (0.11) g/cm^3, while the sheared films (100·s^{-1}) had densities of ~ 1.55 (0.02) g/cm^3. The results suggest that the dried film density increased as CNCs become more oriented, which may be a consequence of the higher packing efficiency of highly anisotropic particles.

Elastic Modulus - The measured values of E as a function of S are shown in Fig. 6a. Unsheared films, with a nearly random in-plane CNC orientation (S=0.04), had an elastic modulus of E=14.9 GPa. This value is much lower than the E=100–220 GPa of individual CNC crystals (in the axial direction), which is considered to be a result of the contributions of both axial and transverse moduli of individual CNCs [49], poor load transfer between CNC particles, and porosity within the film. Shear casting increased the CNC alignment within the direction of the shear (S= 0.27–0.53) and resulted in higher values of E_A (i.e., in the direction of CNC alignment) and greater anisotropy within the film (E_A greater than E_T, which is in the direction transverse to the CNC alignment). The magnitudes of E_A and E_T and the extent of anisotropy (i.e., E_A/E_T) scaled with S at S=0.04 (E=14.9), S=0.27 (E_A=21.5, E_A/E_T ≈2.5), S=0.36(E_A=23, E_A/E_T ≈3.2), and S=0.53 (E_A=29.7, E_A/E_T ≈4.4).

The E≈15 GPa for 2D randomly oriented CNC neat films measured in the current study is higher than previously reported for CNC neat films (wood CNCs, E=6 GPa; tunicate CNCs, E=5–10 GPa) [14–16]. There are several possible causes for the higher E measured in the current study, of which two will be commented on here: film density, and RH during testing. It is assumed here that films with higher density and tested at lower RH will have a higher measured E. In the current study, the film densities were of the order of ~1.4 g/cm^3, which was higher than the 1.2 g/cm^3 used in the Ljungberg et al. [16] study (the other two studies did not report the density of their films). The RH during testing of the current study was ~50%, which was lower than the 65% used by Noiskiki et al. [15] and higher than the ~25% used by Helbert et al. [14] (the other study did not report the RH of testing). Interestingly, the E≈15 GPa of CNC neat films was comparable to values for most BC [1,2,22,24,26] and CNF [17–21,42] neat films with random particle orientation. This is significant because it is

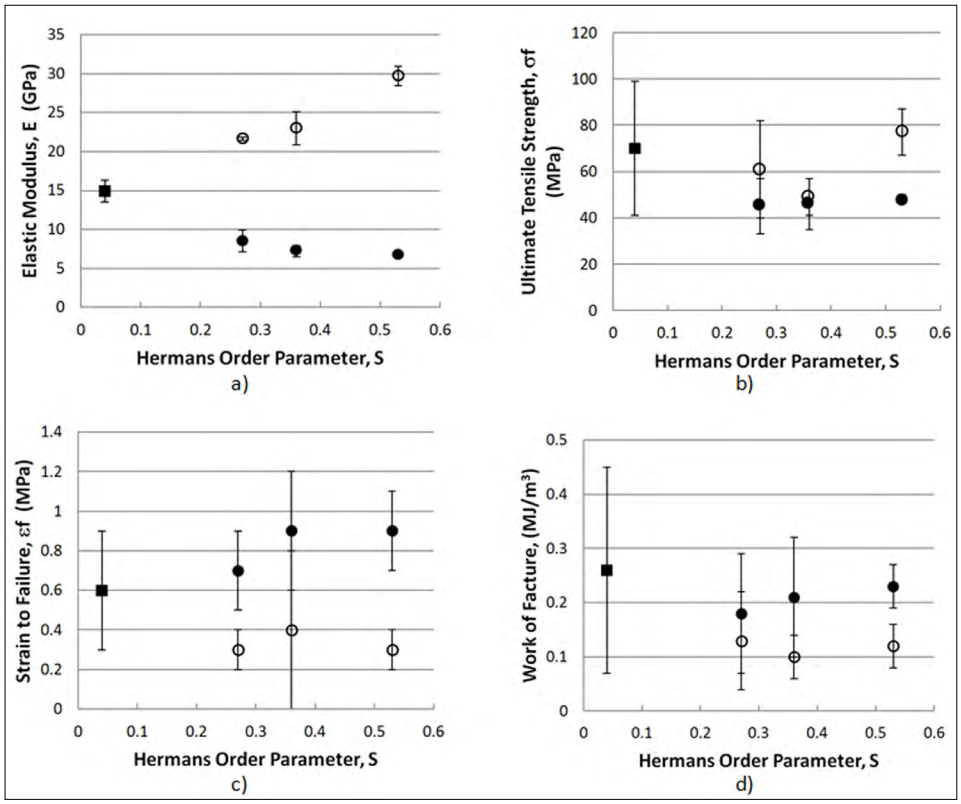

Fig. 6 - Tensile properties verse Hermans order parameter for CNC neat films: a) elastic moduli, b) ultimate tensile strength, c) strain to failure, and d) work of fracture. Sheared films were tested in the axial (open symbols) and transverse (closed symbols) directions with respect to the shearing direction. Unsheared CNC neat films are also tested (filled squares). Error bars are 1 standard deviation.

assumed that the longer BC and CNF particles can produce stronger networks, which then result in stiffer materials.

To the authors' knowledge, the measured $E_A \approx 30$GPa for the CNC aligned film (S=0.53) is the highest value reported for wood-based CNC neat films. This value is also comparable to the highest reported value for all CN neat films (Watanabe et al. [28], BC films, E=28–33 GPa; Nishi et al. [23], BC films, E=30 GPa; and Bohn et al. [22], BC films, E_A=25). In addition, previous studies on CN alignment effects on film mechanical properties did not report the resulting decrease in properties in directions transverse to the CNC alignment direction. In the current study, for the film with S=0.53, the property in the axial direction was $E_A \approx 30$ GPa, but in the transverse direction, it was $E_T \approx 7$ GPa, which is half of that measured for the randomly oriented CNC films (E≈15 GPa).

Tensile Strength, Strain at Failure, and Work of Fracture - The measured, σ_f, ε_f, and WF as functions of S are shown in Figs. 6b, 6c, and 6d respectively. The σ_f = 70 MPa for the unsheared CNC neat films is at the upper end of previously reported studies on CNC neat films (wood CNCs have not been measured previously; only tunicate CNCs films have been measured, σ_f =40–70 MPa) [14–16]. As discussed in the previous section, the films tested in the current study had a higher density, which is one likely reason for the higher σ_f. Incidentally, the σ_f of CNC films are lower than that reported for BC [2,19–24] and CNF [17–21] neat films with random particle orientation and may result from the longer BC and CNF particles producing stronger networks (e.g., more entanglement and particle-particle bonding sites). The value, ε_f=0.6%, was within the range observed by previously reported studies.

CNC alignment is expected to alter σ_f, ε_f, and WF because of the influence of the rod-like particles on the deformation mechanisms of the system. Studies by Bohn et al. [22] and Gindl and Keckes [43] were able to demonstrate that both σ_f and ε_f depend on the degree of CN alignment. In the current study, the role of CNC alignment on σ_f, ε_f, and WF could not be assessed because of the scatter in the data. One exception may be for the CNC-n sample sheared at 100 s^{-1}, in which the lower scatter in the data, combined with the size of the anisotropy within σ_f, ε_f and WF in the axial versus transverse directions, indicates that the high CNC alignment (S=0.53) might be the cause.

Heat Treatment and Film Mechanical Properties

Mechanical properties of CN films typically vary with humidity and thermal history. It was assumed here that residual water alters CNC-CNC interaction within the film and modifies the film mechanical properties. With this in mind, a low-temperature heating step (85°C for 24 h) was used to remove residual water that might be trapped at CNC-CNC interfaces, and the influence of the thermal treatment on properties was then examined. In this case, the thermal treatments of CNC films had minimal influence on E, σ_f, ε_f, and WF. However, the heat treatment did alter the CNC film transparency of the low-pH CNCs by browning the films. The neutral-pH CNC films remained relatively unaffected. It is assumed here that the low-pH films turned dark brown as a result of the increased remnant sulphuric acid further within the films. Sulphuric acid will not evaporate, and therefore any residual amount will concentrate upon drying of the films and break down and dehydrate cellulose.

CONCLUSIONS

The effect of CNC alignment on the resulting mechanical properties (elastic modulus, E, ultimate tensile strength, σ_f, strain to failure, ε_f, and work of fracture, WF) in neat CNC films from wood-based CNCs was investigated. A shear-based solution-casting technique was used to align CNC particles preferentially in the direction of shear within the final dried neat film. The degree of CNC alignment in dried films was found to increase with increasing casting shear rate (0, 10·s^{-1}, and 100·s^{-1}) and higher suspension pH (~3 versus ~7). The highest CNC alignment (S=0.53) was achieved for CNC suspensions with neutral pH at a shear rate of 100·s^{-1}. The influence of CNC alignment was observed on E, but not for σ_f, ε_f, and WF.

Neat CNC films cast without shear had a random 2D CNC orientation within the plane of the film. The measured properties (E≈15 GPa and σ_f = 70 MPa) were higher those previously reported for CNC neat films (wood CNCs, E=6 GPa, σ_f =N/A; tunicate CNCs, E=5–10 GPa, σ_f =40–70 MPa) and were comparable to most BC and CNF neat films with random particle orientation. The maximum E average value measured (E≈30 GPa) was obtained for the neat CNC film with the highest degree of CNC alignment (S=0.53) when measured in the direction of CNC alignment; however, when E was measured in the direction perpendicular to CNC alignment, a much lower value was measured, E≈7 GPa. Thermal treatment (85°C for 24 h) of CNC films altered film transparency, but had minimal influence on tensile properties (E, σ_f, ε_f, and WF).

ACKNOWLEDGMENTS

This work was funded by the U.S. Forest Service-Forest Products Laboratory (FPL). The authors thank Rick Reiner and Alan Rudie of FPL for providing guidance in CNC processing, as well as providing CNC materials.

REFERENCES

1. Moon, R.J., Martini, A., Nairn, J., Simonsen, J., Youngblood, J., "Cellulose Nanomaterials Review: Structure, Properties, and Nanocomposites," Chemical Society Reviews 40(7), 3941-3994 (2011).
2. Iguchi, M., Yamanaka, S., Budhiono, A., "Bacterial Cellulose—A Masterpiece of Nature's Arts," Journal of Materials Science 35(2), 261-270 (2000).
3. Hubbe, M.A., Rojas, O.J., Lucia, L.A., Sain, M., "Cellulosic Nanocomposites: A Review," BioResources 3, 929-980 (2008).
4. Siro, I. and Plackett, D., "Microfibrillated Cellulose and New Nanocomposite

Materials: A Review," Cellulose 17(3), 459-494 (2010).
5. Habibi, Y., Lucia, L.A., Rojas, O.J., "Cellulose Nanocrystals: Chemistry, Self-Assembly, and Applications," Chemical Reviews 110(6), 3479-3500 (2010).
6. Araki, J., Wada, M., Kuga, S., Okana, T., "Influence of Surface Charge on Viscosity Behavior of Cellulose Microcrystal Suspension," Journal of Wood Science 45(3), 258-261 (1999).
7. Araki, J. and Kuga, S., "Effect of Trace Electrolyte on Liquid Crystal Type of Cellulose Microcrystals," Langmuir 17(15), 4493-4496 (2001).
8. Beck-Candanedo, S., Roman, M., Gray, D.G., "Effect of Reaction Conditions on the Properties and Behavior of Wood Cellulose Nanocrystal Suspensions," Biomacromolecules 6(2), 1048-1054 (2005).
9. Dong, X.M., Revol, J.F., Gray, D.G., "Effect of Microcrystallite Preparation Conditions on the Formation of Colloid Crystals of Cellulose," Cellulose 5(1), 19-32 (1998).
10. Elazzouzi-Hafraoui, S., Nishiyama, Y., Putaux, J.L., Heux, L., Dubreuil, F., Rochas, C., "Shape and Size Distribution of Crystalline Nanoparticles Prepared by Acid Hydrolysis of Native Cellulose," Biomacromolecules 9(1), 57-65 (2008).
11. Lima, M.M.D. and Borsali, R., "Rodlike Cellulose Microcrystals: Structure, Properties, and Applications," Macromolecular Rapid Communications 25(7), 771-787 (2004).
12. Lahiji, R.R., Xu, X., Reifenberger, R., Raman, A., Rudie, A., Moon, R.J., "Atomic Force Microscopy Characterization of Cellulose Nanocrystals," Langmuir 26(6), 4480-4488 (2010).
13. Mark, R.E., "Theoretical Strength of the Structural Framework," In Cell Wall Mechanics of Tracheids, Yale University Press: New Haven, 1968; p. 152.
14. Helbert, W., Cavaillé, J.Y., Dufresne, A., "Thermoplastic Nanocomposites Filled with Wheat Straw Cellulose Whiskers, 1. Processing and Mechanical Behavior," Polymer Composites 17(4), 604-611 (1996).
15. Noishiki, Y., Nishiyama, Y., Wada, M., Kuga, S., Magoshi, J., "Mechanical Properties of Silk Fibroin-Microcrystalline Cellulose Composite Films," Journal of Applied Polymer Science 86(13), 3425-3429 (2002).
16. Ljungberg, N., Bonini, C., Bortolussi, F., Boisson, C., Heux, L., Cavaillé, J.Y., "New Nanocomposite Materials Reinforced with Cellulose Whiskers in Atactic Polypropylene: Effect of Surface and Dispersion Characteristics," Biomacromolecules 6(5), 2732-2739 (2005).
17. Henriksson, M., Berglund, L.A., Isaksson, P., Lindstrom, T., Nishino, T., "Cellulose Nanopaper Structures of High Toughness," Biomacromolecules 9(6), 1579-1585 (2008).
18. Saito, T., Hirota, M., Tamura, N., Kimura, S., Fukuzumi, H., Heux, L., Isogai, A., "Individualization of Nano-Sized Plant Cellulose Fibrils by Direct Surface Carboxylation Using TEMPO Catalyst under Neutral Conditions," Biomacromolecules 10(7), 1992-1996 (2009).
19. Henriksson, M. and Berglund, L.A., "Structure and Properties of Cellulose Nanocomposite Films Containing Melamine Formaldehyde," Journal of Applied Polymer Science 106(4), 2817-2824 (2007).
20. Svagan, A.J., Samir, M.A.S.A., Berglund, L.A., "Biomimetic Polysaccharide Nanocomposites of High Cellulose Content and High Toughness," Biomacromolecules 8(8), 2556-2563 (2007).
21. Iwamoto, S., Abe, K., Yano, H., "The Effect of Hemicelluloses on Wood Pulp Nanofibrillation and Nanofibre Network Characteristics.," Biomacromolecules 9(3), 1022-1026 (2008).
22. Bohn, A., Fink, H.P., Ganster, J., Pinnow, M., "X-Ray Texture Investigations of Bacterial Cellulose," Macromolecular Chemistry and Physics 201(15), 1913-1921 (2000).
23. Nishi, Y., Uryu, M., Yamanaka, S., Watanabe, K., Kitamura, N., Iguchi, M., Mitsuhashi, S., "The Structure and Mechanical Properties of Sheets Prepared from Bacterial Cellulose, 2. Improvement of the Mechanical Properties of Sheets and their Applicability to Diaphragms of Electroacoustic Transducers," Journal of Materials Science 25(6), 2997-3001 (1990).
24. Nakagaito, A.N., Iwamoto, S., Yano, H., "Bacterial Cellulose: The Ultimate Nano-Scalar Cellulose Morphology for the Production of High-Strength Composites," Applied Physics a-Materials Science & Processing 80(1), 93-97 (2005).
25. Retegi, A., Gabilondo, N., Pena, C., Zuluaga, R., Castro, C., Ganan, P., de la Caba, K., Mondragon, I., "Bacterial Cellulose Films with Controlled Microstructure-Mechanical Property Relationships," Cellulose 17(3), 661-669 (2010).
26. Yamanaka, S., Watanabe, K., Kitamura, N., Iguchi, M., Mitsuhashi, S., Nishi, Y., Uryu, M., "The Structure and Mechanical Properties of Sheets Prepared from Bacterial Cellulose," Journal of Materials Science 24(9), 3141-3145 (1989).
27. Yamanaka, S., Ishihara, M., Sugiyama, J., "Structural Modification of Bacterial Cellulose," Cellulose 7(3), 213-225 (2000).
28. Watanabe, K., Tabuchi, M., Morinaga, Y., Yoshinaga, F., "Structural Features and Properties of Bacterial Cellulose Produced in Agitated Culture," Cellulose 5(3), 187-200 (1998).
29. Orts, W.J., Godbout, L., Marchessault, R.H., Revol, J.F., "Enhanced Ordering of Liquid Crystalline Suspensions of Cellulose Microfibrils: A Small-Angle Neutron Scattering Study," Macromolecules 31(17), 5717-5725 (1998).
30. Kvien, I. and Oksman, K., "Orientation of Cellulose Nanowhiskers in Polyvinyl Alcohol," Applied Physics a-Materials Science & Processing 87(4), 641-643 (2007).
31. Cranston, E.D. and Gray, D.G., "Formation of Cellulose-Based Electrostatic Layer-By-Layer Films in a Magnetic Field.," Science and Technology of Advanced Materials 7(4), 319-321 (2006).
32. Revol, J.F., Godbout, L., Dong, X.M., Gray, D.G., Chanzy, H., Maret, G., "Chiral Nematic Suspensions of Cellulose

Crystallites—Phase Separation and Magnetic-Field Orientation," Liquid Crystals 16(1), 127-134 (1994).
33. Kimura, F., Kimura, T., Tamura, M., Hirai, A., Ikuno, M., Horii, F., "Magnetic Alignment of the Chiral Nematic Phase of a Cellulose Microfibril Suspension," Langmuir 21(5), 2034-2037 (2005).
34. Sugiyama, J., Chanzy, H., Maret, G., "Orientation of Cellulose Microcrystals by Strong Magnetic Fields," Macromolecules 25(16), 4232-4234 (1992).
35. Habibi, Y., Heim, T., Douillard, R., "AC Electric Field-Assisted Assembly and Alignment of Cellulose Nanocrystals," Journal of Polymer Science Part B-Polymer Physics 46(14), 1430-1436 (2008).
36. Bordel, D., Putaux, J.L., Heux, L., "Orientation of Native Cellulose in an Electric Field," Langmuir 22(11), 4899-4901 (2006).
37. Gindl, W., Emsenhuber, G., Maier, G., Keckes, J., "Cellulose in Never-Dried Gel Oriented by an AC Electric Field," Biomacromolecules 10(5), 1315-1318 (2009).
38. Ebeling, T., Paillet, M., Borsali, R., Diat, O., Dufresne, A., Cavaillé, J.Y., Chanzy, H., "Shear-Induced Orientation Phenomena in Suspensions of Cellulose Microcrystals, Revealed by Small-Angle X-Ray Scattering," Langmuir 15(19), 6123-6126 (1999).
39. Nishiyama, Y., Shigenori, K., Masahisa, W., Takeshi, O., "Cellulose Microcrystal Film of High Uniaxial Orientation," Macromolecules 30(20), 6395-6397 (1997).
40. Hoeger, I., Rojas, O.J., Efimenko, K., Velev, O.D., Kelley, S.S., "Ultrathin Film Coatings of Aligned Cellulose Nanocrystals from a Convective-Shear Assembly System and their Surface Mechanical Properties," Soft Matter 7(5), 1957-1967 (2011).
41. Csoka, L., Hoeger, I.C., Peralta, P., Peszlen, I., Rojas, O.J., "Dielectrophoresis of Cellulose Nanocrystals and Alignment in Ultrathin Films by Electric Field-Assisted Shear Assembly," Journal of Colloid and Interface Science 363(1), 206-212 (2011).
42. Gindl, W., Veigel, S., Obersriebnig, M., Tippelreither, C., Keckes, J., "High-Modulus Oriented Cellulose Nanopaper," In: Functional Materials from Renewable Sources, Liebner, F. (ed.), American Chemical Society: Washington DC, 2012, pp. 1-16.
43. Gindl, W. and Keckes, J., "Drawing of Self-Reinforced Cellulose Films," Journal of Applied Polymer Science 103(4), 2703-2708 (2007).
44. Iwamoto, S., Isogai, A., Iwata, T., "Structure and Mechanical Properties of Wet-Spun Fibres Made from Natural Cellulose Nanofibres," Biomacromolecules 12(3), 831-836 (2011).
45. Reising, A.B., Liu, J.-C., Moon, R.J., Youngblood, J., "Processing of Nanofibrillated and Nanocrystalline Cellulose Neat Films", Proceedings of the International SAMPE Technical Conference, Salt Lake City, UT, (2010).
46. Wada, M., Sugiyama, J., Okano, T., "Native Celluloses on the Basis of Two-Crystalline Phase (I-Alpha/I-Beta) System", Journal of Applied Polymer Science 49(8), 1491-1496 (1993).
47. Hunter, R.J., Introduction to Modern Colloid Science, Oxford University Press: New York, Vol. 1. (1993).
48. Araki, J., Wada, M., Kuga, S., Okano, T., "Birefringent Glassy Phase of a Cellulose Microcrystal Suspension," Langmuir 16(6), 2413-2415 (2000).
49. McCullough, R.L., "Micromechanical Materials Modeling," In: Delaware Composites Design Encyclopedia, Technomic Publishing: Lancaster, Vol. 2, pp. 117-123, (1990).